Chemistry–A European Journal
Research Article
doi.org/10.1002/chem.202400004
Chemistry Europe
European Chemical Societies Publishing
www.chemeurj.org

Aggregation/Crystallization-Induced Emission in Naphthyridine-Based Carbazolyl-Modified Donor-Acceptor Boron Dyes Tunable by Fluorine Atoms

Mykhaylo A. Potopnyk,*[a, b] Justyna Mech-Piskorz,[c] Gonzalo Angulo,*[c] Magdalena Ceborska,[d] Roman Luboradzki,[c] Elina Andresen,[e] Arkadiusz Gajek,[c] Agnieszka Wisniewska,[c] and Ute Resch-Genger*[e]

This paper is dedicated to Professor Sławomir Jarosz

Four donor-acceptor boron difluoride complexes based on the carbazole electron donor and the [1,3,5,2]oxadiazaborinino[3,4-*a*][1,8]naphthyridine acceptor were designed, synthesized, and systematically spectroscopically investigated in solutions, in dye-doped polymer films, and in the solid states. The dyes exhibit an intense blue to red solid-state emission with photoluminescence quantum yields of up to 59% in pure dye samples and 86% in poly(methyl methacrylate) films. All boron complexes show aggregation-induced emission and reversible mechanofluorochromism. The optical properties of these dyes and their solid state luminescence can be tuned by substitution pattern, i.e., the substituents at the naphthyridine unit. Exchange of CH_3- for CF_3-groups does not only increase the intramolecular charge transfer character, but also provides a crystallization-induced emission enhancement.

Introduction

Organic dyes with solid-state emission (SSE)[1] have many applications in material sciences,[2] bioimaging,[3] and supramolecular chemistry.[4] Such dyes can be used as emitters in optoelectronic devices, organic solid-state lasers, security ink, optical probes, and sensors.[5] One SSE mechanism is aggregation-induced emission (AIE),[6] i.e., the introduction of a strong luminescence enhancement due to the formation of dye aggregates by luminogens that are non-emissive or barely emissive in solution. The AIE phenomenon arises from a restricted intramolecular motion (RIM) mechanism, which includes both the restriction of intramolecular rotations (RIR) and the restriction of intramolecular vibrations (RIV). As AIE is related to dye aggregation in solution and the formation of dye nanoparticles and the solid-state emission of organic materials is considerably affected by intermolecular interactions,[7] molecular packing in the crystalline state can significantly affect SSE.[1]

Systematic studies of organic materials revealing solid-state emission reveal that SSE is closely associated with the molecular arrangement, i.e., molecular packing and molecular conformation aspects.[8] Therefore, packing motifs such as π-π-stacking, H- and J-aggregation, or halogen bonding, that can be considerably influenced by substitution pattern, play essential roles in SSE.[9] For example, to prevent π-π stacking, which usually hampers SSE, bulky substituents are often used,[10] while intermolecular hydrogen bonding involving an electron-rich site (such as a halogen, oxygen, nitrogen, or sulfur atom) is

[a] Dr. M. A. Potopnyk
Institute of Organic Chemistry
Polish Academy of Sciences
Kasprzaka 44/52, 01-224, Warsaw (Poland)
E-mail: potopnyk@gmail.com
mykhaylo.potopnyk@icho.edu.pl
Homepage: https://www.icho.edu.pl/en/zespol/mykhaylo-potopnyk-2/

[b] Dr. M. A. Potopnyk
Institute of Organic Chemistry
National Academy of Sciences of Ukraine
Akademika Kuharya Str. 5, 02000, Kyiv (Ukraine)

[c] Dr. J. Mech-Piskorz, Dr. G. Angulo, Dr. R. Luboradzki, Dr. A. Gajek, Dr. A. Wisniewska
Institute of Physical Chemistry, Polish Academy of Sciences
Kasprzaka 44/52, 01-224, Warsaw (Poland)
E-mail: gangulo@ichf.edu.pl
Homepage: https://ichf.edu.pl/en/groups/dynamics-of-light-induced-bimolecular-reactions

[d] Dr. M. Ceborska
Faculty of Mathematics and Natural Sciences
Cardinal Stefan Wyszynski University in Warsaw
K. Woycickiego 1/3, 01-938, Warsaw (Poland)

[e] Dr. E. Andresen, Dr. U. Resch-Genger
Division Biophotonics
Bundesanstalt für Materilaforschung und -prüfung (BAM), Department 1
Richard-Willstätter-Straβe 11, 12489 Berlin (Germany)
E-mail: ute.resch@bam.de
Homepage: https://www.bam.de/Navigation/EN/Home/home.html

Supporting information for this article is available on the WWW under https://doi.org/10.1002/chem.202400004

Research Article
doi.org/10.1002/chem.202400004

known to be an effective way to stabilize the crystal structure of organic materials exhibiting solid-state luminescence.[9b,11]

For some organic materials, such as (4-biphenylyl)phenyldibenzofulvene, 1,2-diphenyl-3,4-bis(diphenylmethylene)-1-cyclobutene, pyrrolidinylvinylquinoxaline derivatives, some boron diiminates, SSE is observed in the crystalline state, but not or only very rarely in the amorphous phase. This effect is referred to as crystallization-induced emission (CIE) or crystallization-induced emission enhancement (CIEE).[12] Nonetheless, the design of SSE materials with an emission solely in the crystalline state is still challenging and calls for an in-depth understanding of the prerequisites for this mechanism. This is very important for the elaboration of CIEE materials. The difference between aggregation and crystallization-induced emission can be caused by different intermolecular interactions including hydrogen bonding.[13] Furthermore, some organic dyes can change their SSE properties upon the application of mechanical forces. This phenomenon is referred to as mechanochromic luminescence or in the case of fluorescent materials, mechanochromic fluorescence (mechanofluorochromism, MFC).[14] MFC results from mechanically induced changes in the molecular conformation or/and intermolecular interactions in the solid state.[15] However, the development of highly emissive MFC materials still remains a major challenge, especially for compounds with an orange and red emission. MFC has been observed for different emitter classes, such as tetraphenylethene[16] and triphenylamine derivatives,[17] chalcones,[18] cyanostylbenes,[19] phenanthroimidazole derivatives,[20] cyclophanes,[21] organophosphonates,[22] and boron difluorides.[11a,e,23]

Herein, we describe the synthesis of a set of donor-acceptor substituted difluoroborine dyes **1**–**4** shown in Figure 1. These dyes are boron complexes with carbazole and di-*tert*-butylcarbazole groups that bear a naphthyridineamide moiety. Carbazole donors are often used in the design of solid-state emissive compounds.[24] Meanwhile naphthyridine-fused oxadiazaborinine (1,1-difluoro-1*H*-1λ[4],11λ[4]-[1,3,5,2]oxadiazaborinino[3,4-*a*][1,8]naphthyridine) scaffold can be used as a strong acceptor in the construction of red-emitting dyes.[25] Multiple fluorine atoms were introduced into these dye structures to enlarge the intermolecular hydrogen bonding ability, thereby aiming for an increase in the solid-state photoluminescence quantum yield (Φ).

The obtained compounds have been thoroughly characterized. This included the assessment of the intermolecular interactions in the solid state of the dyes **1**–**4** to better understand the underlying photophysics also in the aggregate state. In addition, to obtain in-depth information on the electronic structure of boron complexes **1**–**4**, density functional theory (DFT) and time-depended DFT (TD-DFT) calculations were performed. We then assessed the spectroscopic properties of the dyes in liquid solutions, followed by spectroscopic studies of the non-aggregated dyes in more rigid polymer matrices. Then, dye aggregation was explored using THF-water mixtures of varying water content, a solvent, in which the dyes are not soluble. Finally, we studied the photophysics of these fluorophores in the solid states and under influence of mechanical forces.

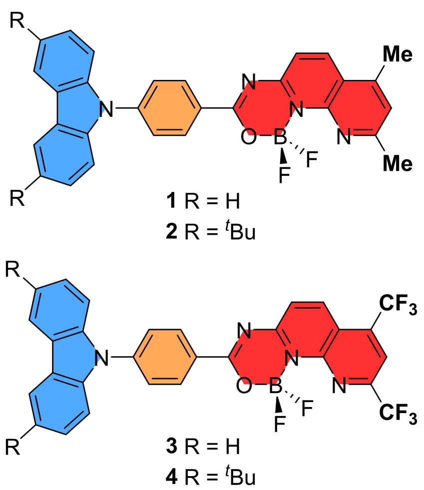

1 R = H
2 R = ^{t}Bu

3 R = H
4 R = ^{t}Bu

Figure 1. Boron complexes **1**–**4**.

Results and Discussion

Synthesis and X-ray crystal determination

The synthesis of the boron complexes **1**–**4** is given in section 2 of the Supporting Information (SI). All boron complexes and precursors were thoroughly characterized by ^{1}H, ^{13}C, and ^{19}F NMR, and high-resolution mass spectrometry (HRMS).

The structures of the crystals of compounds **1**–**4**, obtained from (cyclo)hexane/dichloromethane solutions of the dyes, were confirmed by single-crystal X-ray diffraction studies (Figure S1–S8 in the SI). Compounds **1**, **3**, and **4** form monoclinic crystals of space groups *I*2/*a*, $P2_1/c$, and $P2_1/c$ corresponding to eight, four, and four molecules per unit cell, respectively. Boron complex **2** crystallizes in the triclinic space group *P*-1 with two molecules per unit cell (see Tables S1–S2 in the SI). All compounds show a twisted structure in the crystalline state. The C12-N1-C13-C18 torsion angles between the carbazole unit and phenylene linker of **1**, **2**, **3**, and **4** amount to 43°, −33°, 43°, and −45°, respectively; while the C15-C16-C19-N2 torsion angles between the phenylene linker and the oxadiazaborinine ring show values of about −7°, 12°, −12°, and 7° (Figures 2a, 3a, 4a, 5a, and Table S3 in the SI).

In the crystalline state, compound **1** forms a dye-dichloromethane solvate (with a ratio 1:1). The dye molecules are organized with a "head-to-tail" orientation and are connected to each other by weak n-π/π-π intermolecular interactions (a = 3.322 Å; b = 3.469 Å, Figure 2c) and relatively strong C–H···F hydrogen bonds (c = 2.693 Å, d = 2.471 Å, Figure 2d). Additionally, molecules **1** interact with dichloromethane molecules by C–H···Cl (e = 3.065 Å; f = 2.935 Å, g = 3.000 Å, Figure 2e), C–H···F (h = 2.651 Å, i = 2.637 Å, j = 2.436 Å, Figure 2e), C–H···N (k = 2.686 Å, Figure 2f) hydrogen bonds.

Crystals of derivative **2** contain disordered solvent molecules. Neighbouring dye molecules are also organized in a

Research Article
doi.org/10.1002/chem.202400004

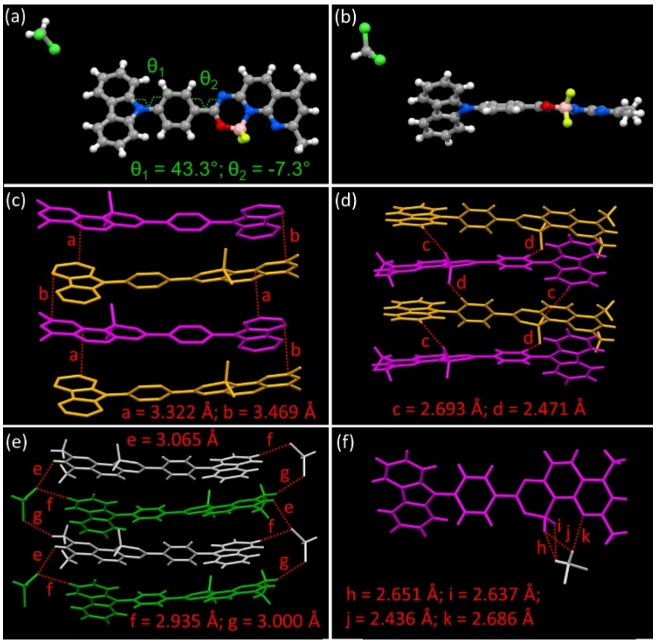

Figure 2. Single crystal analysis of structure **1**: top (a) and front (b) views; intermolecular interactions: n-π and π-π interactions (hydrogen atoms are omitted for clear view) (c); C–H···F hydrogen bonds (d); C–H···Cl hydrogen bonds (e); C–H···F and C–H···N hydrogen bonds (f).

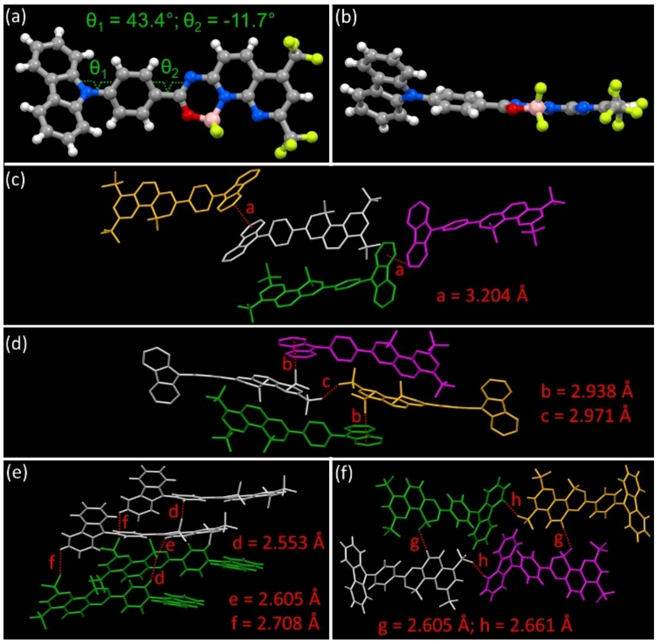

Figure 4. Single crystal analysis of structure **3**: top (a) and front (b) views; intermolecular interactions: π-π interactions (hydrogen atoms are omitted for clear view) (c); F-π and F···F interactions (hydrogen atoms are not shown for clear view) (d); C–H···F hydrogen bonds (e, f).

"head-to-tail" orientation, forming column-like structures by weak n-π/π-π intermolecular interactions (a = 3.594 Å; b = 3.528 Å, Figure 3c), and relatively strong H-π interactions (c = 2.679 Å, Figure 3d) and C–H···F intermolecular hydrogen bonds (d = 2.544 Å, Figure 3d).

The molecular packing of compound **3** is characterized by weak π-π interactions between the carbazole units of neighbouring molecules (a = 3.204 Å, Figure 4c), relatively strong F-π (b = 2.938 Å, Figure 4d) and F···F (c = 2.971 Å, Figure 4d) interactions, as well as multiple C–H···F hydrogen bonds (d = 2.553 Å, e = 2.605 Å, f = 2.708 Å, g = 2.605 Å, h = 2.661 Å, Figures 4e and 4f).

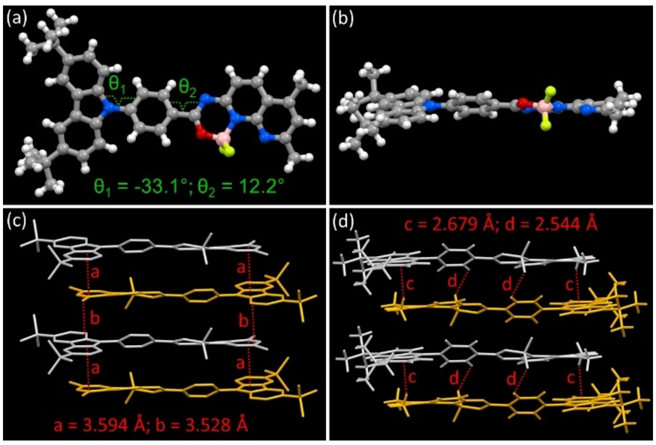

Figure 3. Single crystal analysis of structure **2**: top (a) and front (b) views; intermolecular interactions: n-π and π-π interactions (hydrogen atoms are omitted for clear view) (c); H-π interactions and C–H···F hydrogen bonds (d).

The molecular packing of dye **4** (Figure 5) is affected by the simultaneous presence of the bulky *tert*-butyl and trifluoromethyl groups. The dye molecules form monosolvates with cyclohexane by very weak van der Waals interactions. While the interaction between dye molecules **4** occurs by very small

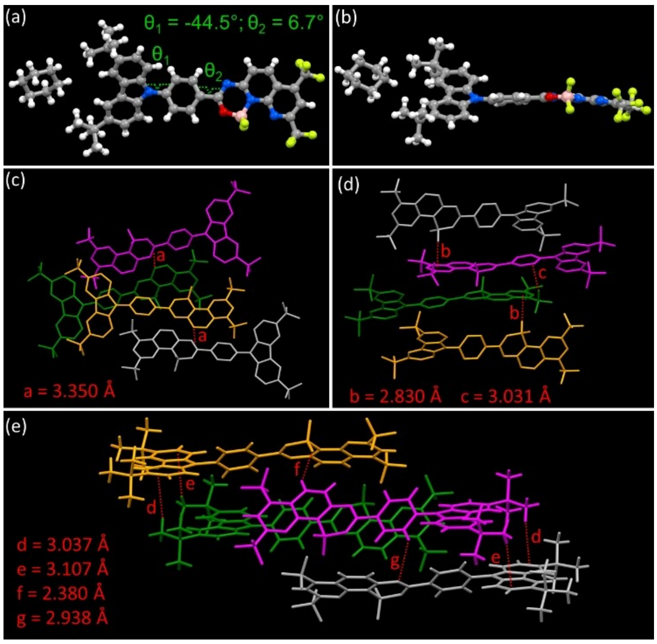

Figure 5. Single crystal analysis of structure **4**: top (a) and front (b) views; intermolecular interactions: n-π/π-π interactions (hydrogen atoms are omitted for clear view) (c); F-π interactions (hydrogen atoms are not shown for clear view) (d); H-π interactions, C–H···F and C–H···N hydrogen bonds (e).

degree of n-π/π-π interactions (a = 3.350 Å, Figure 5c), stronger F-π interactions (b = 2.830 Å, c = 3.031 Å, Figure 5d), weak H-π interactions (d = 3.037 Å, e = 3.107 Å, Figure 5e), as well as, by strong C–H···F (f = 2.380 Å, Figure 5e) and weak C–H···N (g = 2.938 Å, Figure 5e) hydrogen bonds.

Overall, the analysis of crystal packing of the dyes **1**–**4** clearly demonstrates that due to the higher number of fluorine atoms (from the CF_3 and BF_2 groups), molecules **3** and **4** show smaller n-π/π-π interactions (see also Figure S9-S12 in the SI) and stronger hydrogen bond interactions, compared to the CH_3 derivatives **1** and **2**. It should be stressed, that this difference in the intermolecular interactions significantly influences the solid-state photophysical properties of the dyes presented in one of the following sections.

To determine the thermal stability of compounds **1**–**4**, thermogravimetric analysis (TGA) was performed under nitrogen atmosphere in a temperature range of 25–800 °C with a heating rate of 10 °C/min (Figures S13 and S14 in the SI). All boron complexes **1**, **2**, **3**, and **4** show a remarkable thermal stability with decomposition temperatures (T_d) of 340 °C, 318 °C, 319 °C, and 327 °C, respectively.

Quantum chemical calculations

To obtain in-depth information on the electronic structure of the boron dyes **1**–**4**, DFT and TD-DFT calculations were performed at a M06/def2svp level of theory. The solvation in toluene was considered through the conductor-like polarizable continuum model (Figure 6, Table S4 in the SI). The ground-state molecular geometries are characterized by torsion angles between the carbazole unit and *para*-phenylene linker (Θ_1) of 45.2–52.6°, while the position of the naphthyridino-oxadiazaborinine unit with the *para*-phenylene linker is almost coplanar with angles Θ_2 of 0–0.4°. These data correlate well with the single-crystal X-ray data (Figures 2–5). The charge of the highest occupied molecular orbital (HOMO) is mainly located on the carbazole unit, confirming its donor role in these donor-acceptor substituted molecules. The lowest unoccupied molecular orbitals, LUMO and LUMO + 1, are distributed on the planar naphthyridino-oxadiazaborinine unit conjugated with the *para*-phenylene linker, with an essential shift to the naphthyridine part in the case of LUMO, especially for molecules **3** and **4**. These molecular orbital distributions confirm the strong acceptor role of the naphthyridino-oxadiazaborinine unit.

The TD-DFT calculations show that the lowest-energy absorption bands of the investigated dyes correspond to the $S_0 \rightarrow S_1$ transition, which is characterized by a relatively high oscillator strength values of f = 0.568, 0.550, 0.377, and 0.411 for molecules **1**, **2**, **3**, and **4**, respectively. Interestingly, the $S_0 \rightarrow S_1$ excitation has mainly HOMO→LUMO character for compounds **3** and **4**, and mixed HOMO→LUMO/HOMO→LUMO + 1 character for analogues **1** and **2**. The electron distributions on HOMO, LUMO and LUMO + 1 (Figures 6 and Table S4 in the SI) indicate that the lowest-energy absorption band can be attributed to the intramolecular charge transfer (ICT) transition.

Photophysical properties in solutions

The absorption and photoluminescence properties of dyes **1**–**4** were first studied in toluene using a dye concentration c of

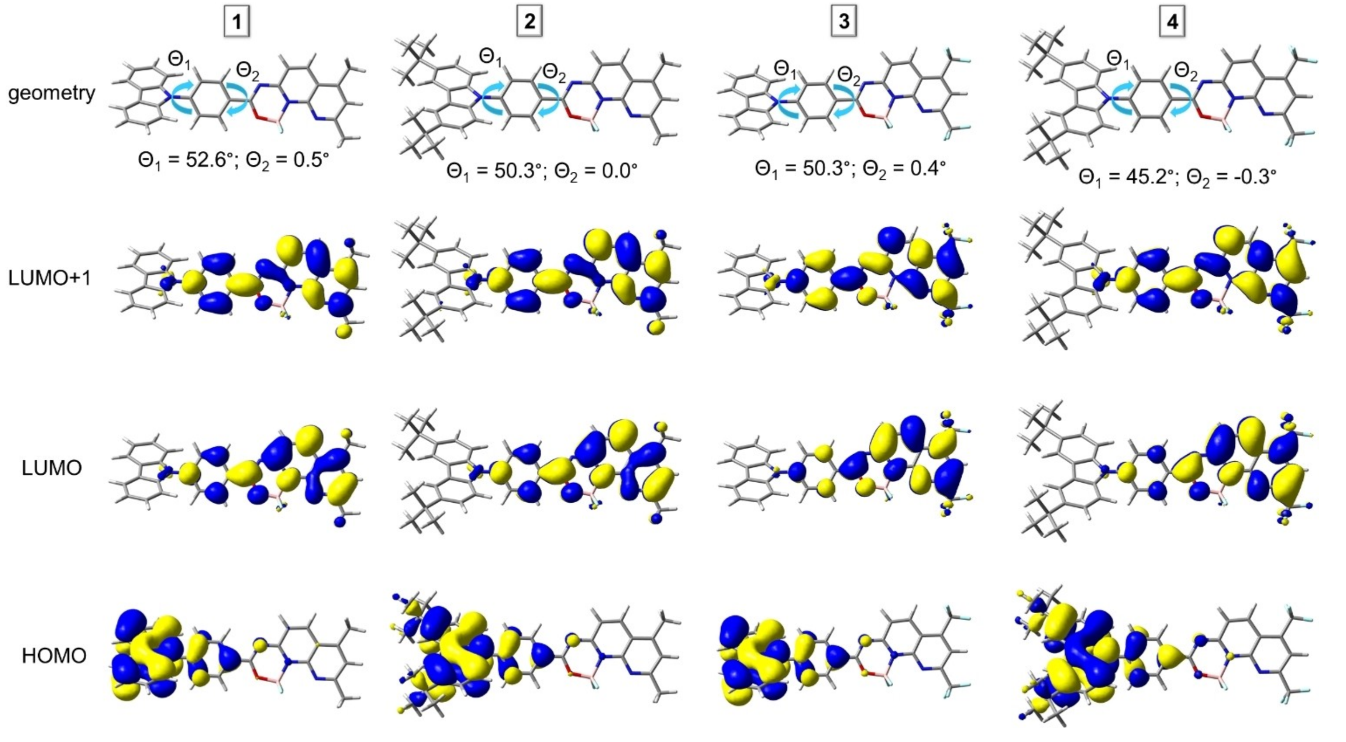

Figure 6. Optimized ground-state structures and HOMO, and Franck-Condon LUMO and LUMO + 1 of compounds **1**–**4**.

Research Article
doi.org/10.1002/chem.202400004

1×10^{-5} M. The lowest-energy ($S_0 \rightarrow S_1$ transition) absorption bands peak at 412 nm, 427 nm, 451 nm, and 474 nm for dyes **1**, **2**, **3**, and **4**, respectively (Figure 7). These data correlate well with the theoretical calculations (Table S4 in the SI).

The photoluminescence properties of the compounds in toluene are affected by the electron donor/acceptor strengths of the carbazole/oxadiazaborinino-naphthyridine units. Compounds **1** and **2** with CH_3 substituents at the naphthyridine unit show a very intense fluorescence with emission maxima at 467 nm and 488 nm, and fluorescence quantum yields Φ of 0.78–0.79. The emission decay kinetics of the toluene solutions of both dyes are monoexponential and provide lifetimes (τ) ranging from 3 ns to 7 ns. The rate constants for radiative (k_r) deactivation amount to $2.56\times10^8\ s^{-1}$ and $1.85\times10^8\ s^{-1}$ for dyes **1** and **2**, thereby exceeding the corresponding constants for non-radiative (k_{nr}) deactivation of $6.8\times10^7\ s^{-1}$ and $5.2\times10^7\ s^{-1}$ (Table S5 in the SI) by a factor of more than 3.5. In the case of the CF_3-modified derivatives **3** and **4**, the emission bands are bathochromically shifted to 560 nm and 597 nm, and the fluorescence quantum yields are decreased to 0.53 and 0.21. The value of k_{nr} of $6.9\times10^7\ s^{-1}$ is comparable with that of k_r of $7.8\times10^7\ s^{-1}$ for **3** in toluene and increased for the toluene solution of compound **4** ($k_{nr} = 2.04\times10^8\ s^{-1}$, $k_r = 5.4\times10^7\ s^{-1}$). This suggests that the increasing acceptor strength of the naphthyridine unit, and the accordingly increased donor-acceptor character in compounds **1**–**4** accounts for the red shift of the emission spectra and the concomitant increase of the non-radiative depopulation of the excited singlet state of the dyes.

To shed more light on the luminescence features of dyes **1**–**4** the absorption and photoluminescence spectra of these compounds were subsequently explored in different solvents of varying polarity, i.e., hexane, chloroform, dichloromethane, acetone, and acetonitrile (Table S5 and Figures S15-S22, see SI). These studies reveal that the absorption spectra of the dyes are not significantly affected by solvent polarity. An increase in solvent polarity causes a slight hypsochromic shift of the absorption band, which is most pronounced for acetone and acetonitrile solutions. Only in apolar hexane, a slight vibrational fine structure of the absorption spectra can be observed. Contrary, the emission properties of dyes **1**–**4** are significantly influenced by solvent polarity.

In hexane, as the least polar solvent used here, the emission maxima λ_{em} of all dyes are hypsochromically shifted, yielding λ_{em} values of 424 nm, 442 nm, 478 nm, and 513 nm for dyes **1**, **2**, **3**, and **4**, respectively, in comparison to the respective emission maxima in toluene solutions. The Φ values range from 0.70 to 0.81, making even the CF_3 derivatives **3** and **4** highly emissive in this apolar solvent. The lifetimes range from 1.77 ns for compound **1** to 6.29 ns for dye **4** (Table S5 in the SI), thereby increasing with increasing CT character of the dye. This yields k_r values of the dyes in the order of **1** ($3.95\times10^8\ s^{-1}$) $>$ **2** ($3.25\times10^8\ s^{-1}$) $>$ **3** ($1.98\times10^8\ s^{-1}$) $>$ **4** ($1.29\times10^8\ s^{-1}$). While the k_{nr} values are much smaller for each dye solution ($1.69\times10^8\ s^{-1}$, $7.6\times10^7\ s^{-1}$, $5.9\times10^7\ s^{-1}$, and $3.0\times10^7\ s^{-1}$ for compounds **1**, **2**, **3**, and **4**, respectively).

In more polar solvents, the emission bands of all boron dyes lose their fine structure and undergo considerable bathochromic shifts with a concomitant decrease of the Φ value. Thus, in medium polar chloroform/dichloromethane solutions, the emission maxima shift to 510/542 nm and 553/589 nm for CH_3-derivatives **1** and **2**. The corresponding Φ values decrease to 0.46/0.37 and 0.39/0.14. While the lifetimes of the excited state are in the range of 3.9–7.3 ns. As a consequence, the rate constants for the non-radiative deactivation ($9.6\times10^7\ s^{-1}$ and $8.4\times10^7\ s^{-1}$ for chloroform solutions, and $8.6\times10^7\ s^{-1}$ and $2.29\times10^7\ s^{-1}$ for dichloromethane solutions of boron complexes **1** and **2**, respectively) are slightly higher than the corresponding radiative constants ($8.2\times10^7\ s^{-1}$ and $5.3\times10^7\ s^{-1}$ for chloroform solutions, and $5.1\times10^7\ s^{-1}$ and $3.6\times10^7\ s^{-1}$ for dichloromethane solutions of compounds **1** and **2**, respectively). In sharp contrast, the solutions of CF_3-analogus **3** and **4** in chloroform/dichloromethane demonstrate a miserable fluorescence efficiency ($\Phi \leq 0.02$) accompanied by large bathochromic shifts ($\lambda_{em} = 619/655$ nm and 657/617 nm for dyes **3** and **4**, respectively, Table S5 in the SI).

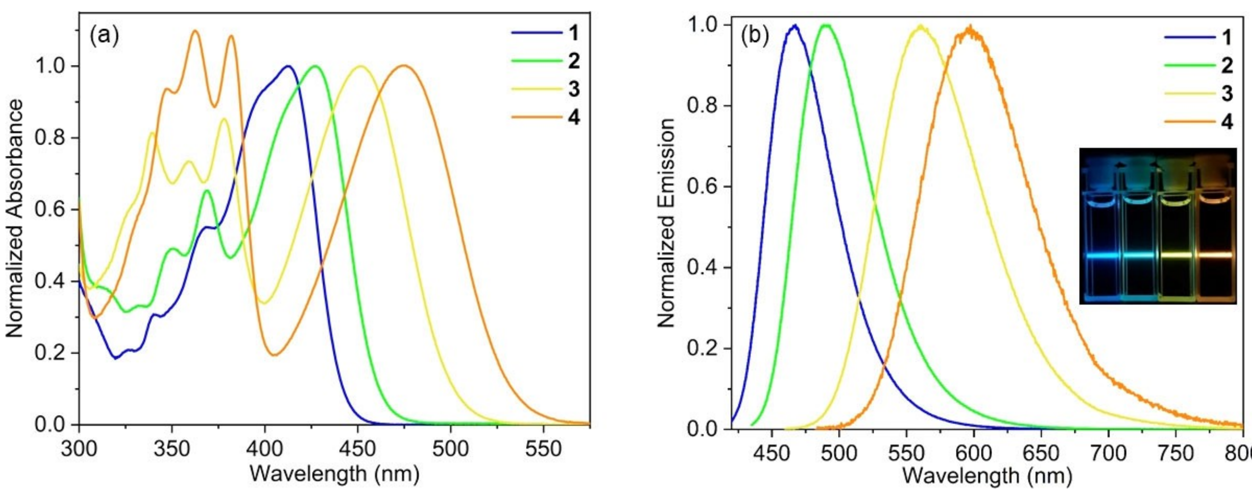

Figure 7. Absorption (a) and emission (b) spectra of compounds **1**–**4** in toluene.

This tendency is even more pronounced in the case of high-polar acetone and acetonitrile solutions. Compounds **1** and **2** show a large red shift of the emission spectra (λ_{em} = 578/605 nm and 612/630 nm, respectively in acetone/acetonitrile solutions) with weak photoluminescence quantum yields (0.06/0.01 and 0.02/< 0.01) and low lifetimes of the excited state (1.31/0.31 ns and 0.38/0.43 ns, respectively). This corresponds to much increased non-radiative decay constants (k_{nr} = 0.7×10^9/3.2×10^9 s^{-1} and 2.6×10^9/> 2.3×10^9 s^{-1}) exceeding the respective radiative decay rates (k_r = 4.6×10^7/3.2×10^7 s^{-1} and 5.3×10^7/< 2.3×10^7 s^{-1}). Meanwhile, CF_3-analogues **3** and **4** are basically non-emissive in acetone and acetonitrile solutions (Table S5 in the SI).

The bathochromic shifts of the emission bands with increasing solvent polarity indicate that the excited state (ES) dipole moment is larger than the dipole moment in the ground state (GS). This could suggest the formation of non-emissive twisted intramolecular charge transfer (TICT) states,[26] especially for compounds **3** and **4** in polar solvents. A simplified Jablonski diagram is depicted in Figure 8 that roughly explains the spectral shifts in absorption and emission observed for dyes **1**–**4** as a function of solvent polarity.

More information about the absorption and emission properties of boron complexes **1**–**4** in solutions is presented in section 6 of the SI.

Photoluminescence properties in polymeric matrix

Having in hand the photophysical properties of compounds **1**–**4** in solutions, we decided to investigate also their luminescent properties in a rigid matrix, in which the intramolecular rotations of the dye molecule are restricted. As the matrix, low-polar transparent poly(methyl methacrylate) (PMMA) was selected. To suppress intermolecular interaction between the dye molecules, we used a small percentage of the emitter in the PMMA matrix film. To achieve this, the neat films were prepared by doping 1% of a dye in PMMA using spin-coating techniques.

The emission properties of such films can be compared with those of low-polar toluene solutions. Thus, the doped films of dyes **1**, **3**, and **4** demonstrate hypsochromically shifted emission peaks (λ_{em} = 461 nm, 541 nm, and 559 nm for dyes **1**, **3**, and **4**, respectively), while the analogical film of compound **2** exhibits bathochromically shifted broader peak maximized at 502 nm (Figure 9) in comparison with corresponding toluene solutions. While the photoluminescence quantum yield values of these films (Φ = 0.82, 0.86, 0.71, and 0.43 for dyes **1**, **2**, **3**, and **4**, respectively) are higher than those of the toluene solutions. The average lifetimes of the dye-doped PMMA samples are determined to be 3.4 ns, 5.5 ns, 8.2 ns, and 7.4 ns for boron complexes **1**, **2**, **3**, and **4**, respectively. This results in the increase of the k_r value and the decrease of the k_{nr} values as compared with those of toluene solutions of all four dyes (Tables S5 and S6 in the SI).

Thereby due to the efficient RIR, the radiative processes in the dye-doped PMMA films are much higher than those in the corresponding diluted toluene solutions. This data demonstrates that the investigated dyes are highly emissive also in diluted rigid environments.

Aggregation-induced emission

To examine the occurrence of AIE, the photophysical properties of dyes **1**–**4** were investigated in THF-water mixtures containing different volume fractions (f_w) of water.

As follows from Figure 10 and Figure S30 in the SI, for f_w increased from 0 to 20%, compounds **1** and **2** show a drastic decrease of their emission intensity accompanied by a bathochromic shift in the emission bands. This behaviour correlates with the assumed CT character of these dyes, since the increasing water amount in the THF/water mixture results in an increase of the polarity of the dye microenvironment. However,

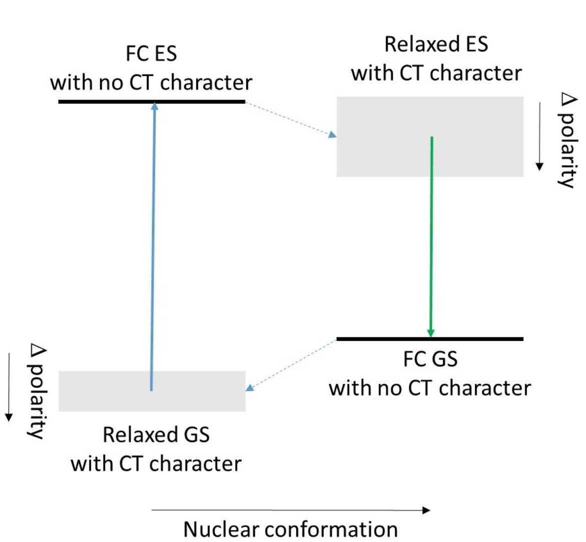

Figure 8. Simplified Jablonski diagram for dyes **1**–**4**. (GS – ground state; ES – excited state; CT- charge transfer; FC ES – Franck-Condon excited state; FC GS – neutral Franck-Condon ground state).

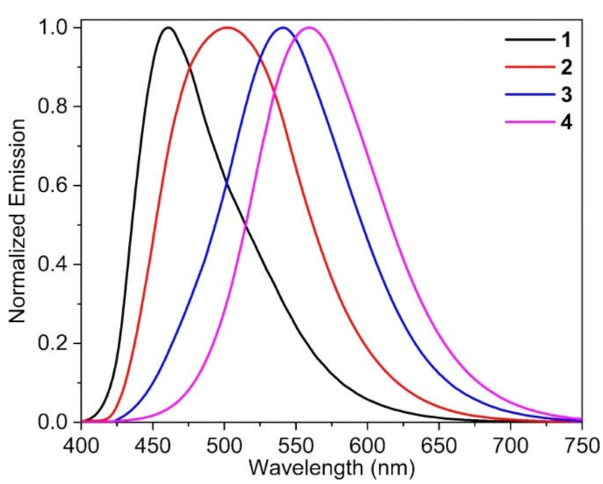

Figure 9. Photoluminescence spectra of doped thin films of compounds **1**–**4** in PMMA (1% of dye).

Research Article
doi.org/10.1002/chem.202400004

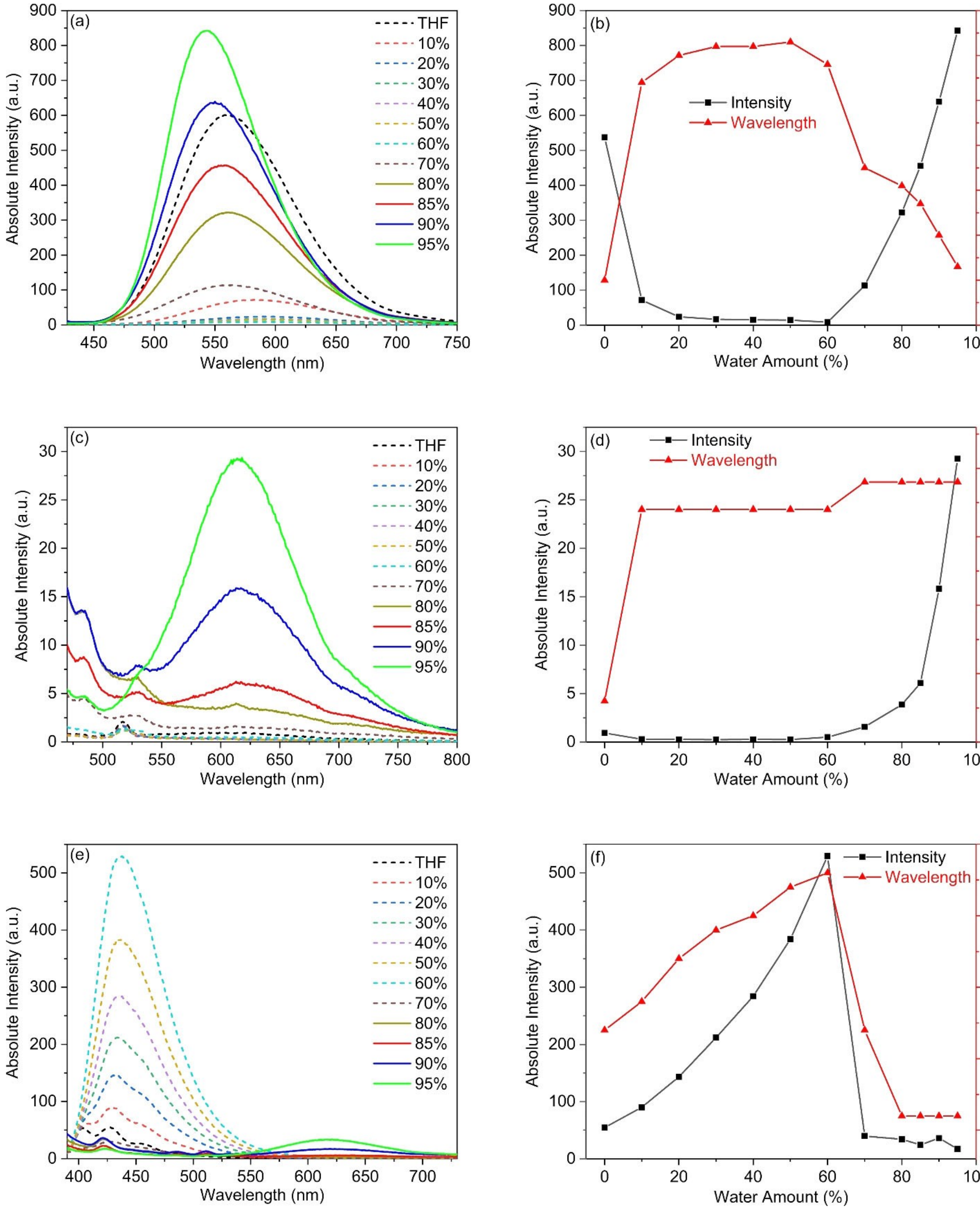

Figure 10. a, c, e: Fluorescence spectra of solutions of dyes **2** (a, $\lambda_{ex}=414$ nm) and **4** (c, $\lambda_{ex}=450$ nm; e, $\lambda_{ex}=375$ nm) in THF/water mixtures of varying water content. The dye concentration used was 1.0×10^{-5} M. b, d, f: Plots of emission intensity (black) and emission maximum (red) of dyes **2** (b, $\lambda_{ex}=414$ nm) and **4** (d, $\lambda_{ex}=450$ nm; f, $\lambda_{ex}=375$ nm, for first higher-energy emission peak) versus f_w.

for dye solutions with $f_w \geq 70\%$, we observed a different behaviour, i.e., an increase of the fluorescence intensity together with a hypsochromic shift of the emission band. These observations are ascribed to the AIE, and the formation of dye aggregates. Compound **2**, with its bulky *tert*-butyl substituents, shows a more pronounced AIE effect compared to dye **1**. The emission maximum of the higher aqueous sample of boron complexes **1** ($\lambda_{em}=496$ nm) is analogical to that of its crystalline sample (see Table 1 in the next section), indicating the formation of microcrystals during the aggregation in THF/water environment. In contrast, the emission peak of *tert*-butyl analogue **2** in THF/water sample with $f_w = 95\%$ is maximised at 543 nm, which is the mean between the corresponding values of crystalline ($\lambda_{em} = 529$ nm) and amorphous ($\lambda_{em} = 557$ nm) samples of this dye (see Table 1). This can indicate that during the aggregation compound **2** forms the mixed crystalline/amorphous particles.

The CF_3 derivatives **3** and **4**, which represent weak emission in medium-polarity solvents, show a slight decrease of the fluorescence with a change in solvent polarity for THF and THF/water mixtures ($f_w = 10$–60%). This is in line with the solvatofluorochromic effect, described above. When the water fraction is increased above 70%, the fluorescence intensity increases, and the emission maximum is bathochromically shifted from 543 nm to 601 nm for dye **3** (Figure S30c,d in the SI) and from 612 nm to 614 nm for dye **4** (Figure 10c,d). This supports also AIE for these boron complexes. However, contrary to dyes **1** and **2**, in the case of compounds **3** and **4**, the AIE-related fluorescence intensity enhancement is much lower. This is tentatively ascribed to an unfavourable molecular conformation and intermolecular interactions in the dye particles formed upon dye aggregation in solutions with a high water fraction. This seems to be favoured by the larger molecular dipoles of the CF_3 derivatives. The luminescence maxima of the highly aqueous samples of these two compounds are approximated to those of corresponding amorphous solid samples ($\lambda_{em} = 609$ nm and 620 nm for dyes **3** and **4**, respectively), indicating the amorphous nature of the formed aggregates.

Interestingly, the excitation of compounds **3** and **4** dissolved in THF/water mixtures of varying water content at the second absorption peaks ($\lambda_{ex} = 370$ nm for dye **3** and $\lambda_{ex} = 375$ nm for dye **4**) results in a blue shift of the emission, located at $\lambda_{em} =$ 430-440 nm for dye **3** and $\lambda_{em} = 428$-436 nm for dye **4**. The intensity of this higher-energy emission increases with increasing water amount up to a water fraction of 60% and drastically decreases when the dye molecules start to aggregate ($f_w = 70$-95%). This effect was not observed for CH_3 derivatives **1** and **2**.

Table 1. Photoluminescence properties of dyes **1**–**4** in the solid states.

Dye	State	λ_{em}, nm[a]	Φ[b]	τ, ns[c]
1	Crystalline	496	0.30	1.12[d]
	Ground	537	0.59	2.85[d]
	DCM-fumed	498	0.23	2.25[d]
	Non-doped film	541	0.08	10.2[d]
2	Crystalline	529	0.17	2.41[d]
	Ground	557	0.39	3.53[d]
	DCM-fumed	529	0.15	2.37[d]
	Non-doped film	557	0.13	1.2[d]
3	Crystalline	569	0.18	47.96[d]
	Ground	609	0.03	4.98[d]
	DCM-fumed	566	0.06	17.35[d]
	Non-doped film	614	0.02	5.5[d]
4	Crystalline	576	0.34	8.29[e]
	Ground	620	0.05	2.44[e]
	DCM-fumed	571	0.21	4.54[e]
	Non-doped film	633	0.01	3.7[e]

[a] Emission maximum. [b] Photoluminescence quantum yield. [c] Average excited-state lifetime. [d] Excited at 375 nm. [e] Excited at 450 nm.

Photophysical properties in the solid state

At first, we investigated the solid-state luminescence properties of boron complexes **1**–**4** in crystalline samples. In the pristine crystalline state compounds **1** and **2** show a broad emission centred at 496 nm and 529 nm, respectively. Crystalline CF_3 derivatives **3** and **4** show bathochromically shifted emission spectra with maxima at 569 nm and 576 nm, respectively (Figure 11). The Φ values of these samples were determined to 0.30, 0.17, 0.18, and 0.34 for compounds **1**, **2**, **3**, and **4**, respectively (Table 1).

Next, we investigated the influence of mechanical forces on the SSE properties. The pristine crystalline samples were ground by hand with a spatula, and the emission spectra were recorded. All ground samples revealed red-shifted emission spectra with respect to those of the initially untreated crystalline samples. Additionally, the Φ values of the ground CH_3-containing compounds **1** and **2** increased to values of 0.59 and 0.39. The CF_3-modified complexes **3** and **4** revealed the opposite behaviour, i.e., a considerable decrease of Φ to values of 0.03 and 0.05. Of note, the average excited state lifetime of the solid samples were increased in the case of CH_3-containing compounds (from 1.12 ns to 2.85 ns, and from 2.41 ns to 3.53 ns, for dyes **1** and **2**, respectively) and decreased in the case of CF_3-derivatives (from 47.96 ns to 4.98 ns, and from 8.29 ns to 2.44 ns for dyes **3** and **4**, respectively) after grinding. This suggests that the incorporation of additional fluorine atoms (dyes **3** and **4**) in the structure of the investigated fluorophores reverses the ratio of radiative/non-radiative processes before and after grinding.

Interestingly, in the presence of dichloromethane (DCM) vapour, we observed the recovery of the initial SSE properties of the samples. The samples treated with DCM vapour demonstrated almost identical emission spectra as the initially used crystalline samples prior to grinding (Figure 11), and the same Φ values.

Subsequently, we assessed the reversibility of the MFC-induced changes in fluorescence of all four dyes under repeated ground/DCM-fuming cycles (Figure S36, the SI). This suggests the occurrence of CIEE in the case of compounds **3** and **4**, in contrary to analogues **1** and **2**. More details about the photoluminescence properties of compounds **1**–**4** in the solid-state are located in section 9 of the SI.

To elucidate the SSE properties of **1**–**4**, we performed powder X-ray diffraction (PXRD) measurements of the pristine crystalline and, ground samples and the samples treated with DCM fume (Figure S38 in the SI). The analysis of PXRD patterns reveals the occurrence of crystalline-to-amorphous and amor-

Chemistry Europe
European Chemical Societies Publishing

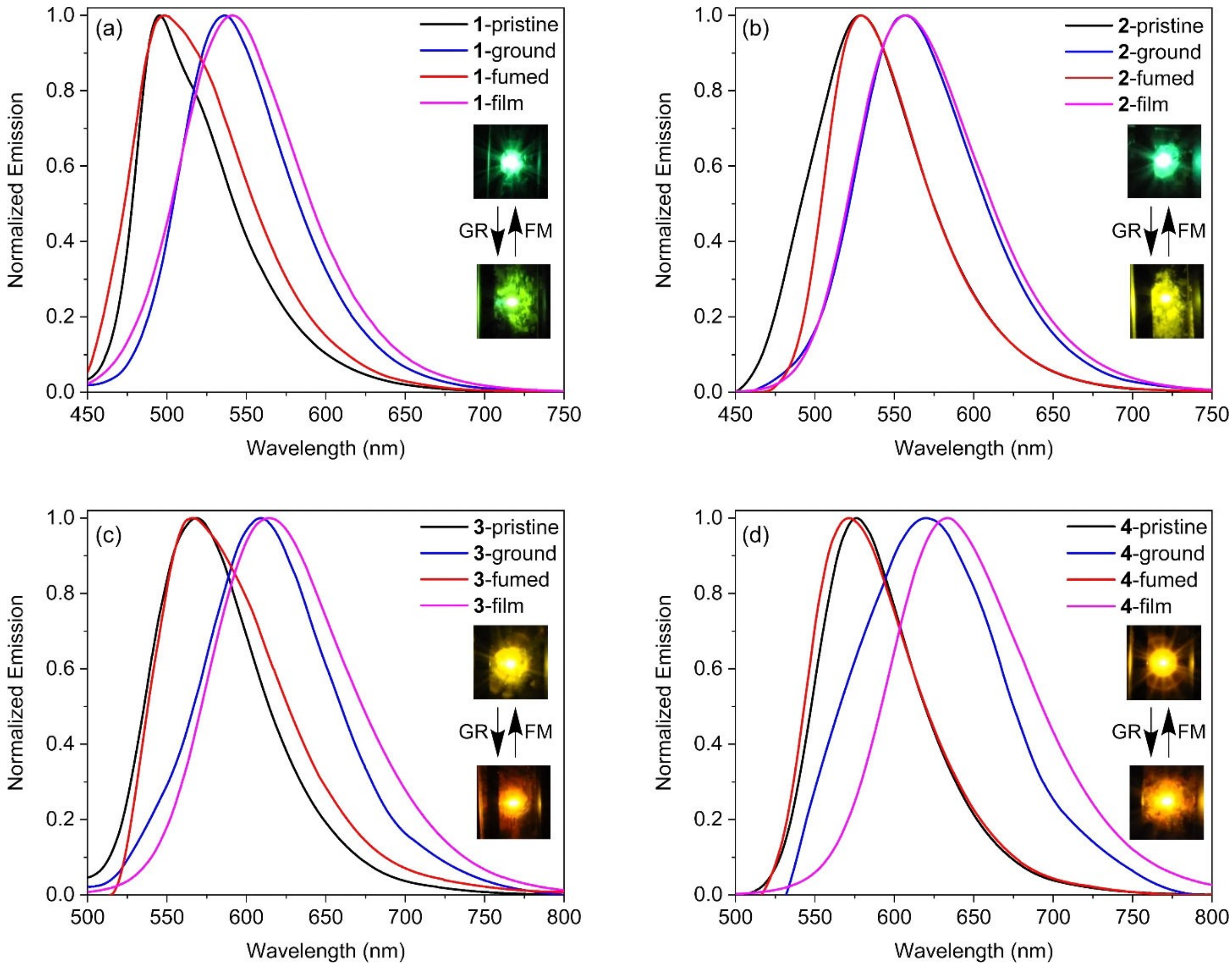

Figure 11. Normalized emission spectra of compounds **1** (a), **2** (b), **3** (c) and **4** (d) in pristine crystalline (black), ground (blue), and DCM-fumed (red) states, as well as non-doped thin films (magenta). Inset: the photographs of pristine crystalline and grinded solid samples of compounds **1**–**4** under a 375 nm UV light illumination.

phous-to-crystalline morphological transitions during the grinding and DCM-fuming processes. This suggests that to induce the SSE of dyes **3** and **4**, well-aligned molecular packing is required which suppresses bond rotations. On the contrary, in the case of compounds **1** and **2**, the SSE is more intense in the amorphous state; hence, SSE enhancement factor is the breaking of intermolecular interactions. Given that the crystal packing of compounds **3** and **4** includes stronger hydrogen bond interactions and smaller n-π/π-π interactions in comparison to those o CH_3 analogues **1** and **2** (Figures 2–5), we conclude that the SSE properties of such dyes can be tuned by the fluorine atoms. Despite the fact that the incorporation of CF_3 groups in the molecular structure drastically decreases the luminescence in solutions because of the increase of acceptor character of naphthyridino-oxadiazaborinine unit, it plays the opposite role in the crystalline state: due to the ability to form multiple C–H···F hydrogen bond interactions, fluorine atoms stabilize the molecular packing without a significant n-π/π-π interactions and increase the SSE.

Finally, we examined non-doped films of these dyes. The emission spectra of the non-doped films of compounds **1**–**4** reveal emission bands at 541 nm, 557 nm, 614 nm, and 633 nm, respectively, and are almost identical with the emission spectra of the corresponding ground samples (Figure 11). These results suggest that in the non-doped films the compounds are in the amorphous state.

Conclusion and outlook

We designed, synthesized, and spectroscopically investigated four donor-acceptor boron difluoride dyes **1**–**4** constituted of a carbazole electron donor and a [1,3,5,2]oxadiazaborinino[3,4-*a*][1,8]naphthyridine acceptor. Spectroscopic studies of these dye molecules in aprotic solvents of varying polarity reveal a red shift in the emission spectra and a diminution in fluorescence intensity in acetone and acetonitrile solutions. The solid-state luminescence of the dyes can be tuned by intermolecular interactions, especially C–H···F hydrogen bonding. Apparently, the presence of CF_3 groups in compounds **3** and **4** is responsible for the crystallization-induced emission enhancement observed for these dyes. Overall, our work sheds new light on the design of CIEE and AIE phenomena. To further deepen our understanding of the photophysics of this dye class, new boron difluoride dyes consisting of triarylamine donor groups and [1,3,5,2]oxadiazaborinino[3,4-*a*][1,8]naphthyridine acceptors are currently being prepared for further spectroscopic studies and applications in functional materials.

Supporting Information

Experimental procedures and characterization data. ORTEP diagrams for the X-ray structures and crystal data of complexes. Details of computational work. Thermal analysis. Additional photophysical data in solutions and the solid states. NMR spectra.

Deposition Numbers CCDC 2128405 (for **1**), CCDC 2128406 (for **2**), CCDC 2128407 (for **3**), CCDC 2291262 (for **4**) contain the supplementary crystallographic data for this paper. These data are provided free of charge by the joint Cambridge Crystallographic Data Centre and Fachinformationszentrum Karlsruhe Access Structures service. The authors have cited additional references within the Supporting Information.[27–41]

Acknowledgements

This work was supported by the "Long-term program of support of the Ukrainian research teams at the Polish Academy of Sciences carried out in collaboration with the U.S. National Academy of Sciences with the financial support of external partners". We gratefully acknowledge Polish high-performance computing infrastructure PLGrid (HPC Centers: WCSS) for providing computer facilities and support within computational grant no. PLG/2021/015105. We are also grateful to Prof. Jacek Waluk from the Institute of Physical Chemistry of the Polish Academy of Sciences for fruitful discussions. Open Access funding enabled and organized by Projekt DEAL.

Conflict of Interests

The authors declare no conflict of interest.

Data Availability Statement

Research data are not shared.

Keywords: solid-state luminescent emission · aggregation-induced emission · mechanochromic luminescence · stimuli-responsive materials · boron difluoride complex

[1] a) J. Gierschner, J. Shi, B. Milián-Medina, D. Roca-Sanjuán, S. Varghese, S. Y. Park, *Adv. Opt. Mater.* **2021**, *9*, 2002251; b) S. K. Behera, S. Y. Park, J. Gierschner, *Angew. Chem. Int. Ed.* **2021**, *60*, 22624–22638; c) A. Huber, J. Dubbert, T. D. Scherz, J. Voskuhl, *Chem. Eur. J.* **2023**, *29*, e202202481.
[2] X. Cai, B. Liu, *Angew. Chem. Int. Ed.* **2020**, *59*, 9868–9886.
[3] A. Chaudhuri, A. Paul, A. Sikder, N. D. P. Singh, *Chem. Commun.* **2021**, *57*, 1715–1733.
[4] T. L. Mako, J. M. Racicot, M. Levine, *Chem. Rev.* **2019**, *119*, 322–477.
[5] J. Zhang, B. He, Y. Hu, P. Alam, H. Zhang, J. W. Y. Lam, B. Z. Tang, *Adv. Mater.* **2021**, *33*, 2008071.
[6] a) Y. Hong, J. W. Y. Lam, B. Z. Tang, *Chem. Soc. Rev.* **2011**, *40*, 5361–5388; b) J. Mei, N. L. C. Leung, R. T. K. Kwok, J. W. Y. Lam, B. Z. Tang, *Chem. Rev.* **2015**, *115*, 11718–11940; c) K. Kokado, K. Sada, *Angew. Chem. Int. Ed.* **2019**, *58*, 8632–8639; d) F. Wurthner, *Angew. Chem. Int. Ed.* **2020**, *59*, 14192–14196; e) Z. Zhao, H. Zhang, J. W. Y. Lam, B. Z. Tang, *Angew. Chem. Int. Ed.* **2020**, *59*, 9888–9907; f) L. Biesen, N. Nirmalananthan-Budau, K. Hoffmann, U. Resch-Genger, T. J. J. Müller, *Angew. Chem. Int. Ed.* **2020**, *59*, 10037–10041.
[7] a) C. Lv, W. Liu, Q. Luo, H. Yi, H. Yu, Z. Yang, B. Zou, Y. Zhang, *Chem. Sci.* **2020**, *11*, 4007–4015; b) K. Pauk, S. Lunak Jr., A. Ruzicka, A. Markova, A. Mausova, M. Kratochvil, K. Melanova, M. Weiter, A. Imramovsky, M. Vala, *Chem. Eur. J.* **2021**, *27*, 4341–4348; c) D. Liu, F. Zhu, D. Yan, *J. Mater. Chem. C* **2022**, *10*, 2663–2670; d) R. Huang, C. Wang, D. Tan, K. Wang, B. Zou, Y. Shao, T. Liu, H. Peng, X. Liu, Y. Fang, *Angew. Chem. Int. Ed.* **2022**, *61*, e202211106.
[8] a) A. Wakamiya, K. Mori, S. Yamaguchi, *Angew. Chem. Int. Ed.* **2007**, *46*, 4273–4276; b) K. Wang, H. Zhang, S. Chen, G. Yang, J. Zhang, W. Tian, Z. Su, Y. Wang, *Adv. Mater.* **2014**, *26*, 6168–6173; c) K. Guo, F. Zhang, S. Guo, K. Li, X. Lu, J. Li, H. Wang, J. Cheng, Q. Zhao, *Chem. Commun.* **2017**, *53*, 1309–1312; d) M.-J. Sun, Y. Liu, W. Zeng, Y. S. Zhao, Y.-W. Zhong, J. Yao, *J. Am. Chem. Soc.* **2019**, *141*, 6157–6161; e) S. Yokoyama, N. Nishiwaki, *J. Org. Chem.* **2019**, *84*, 1192–1200; f) C. Zhang, X. Wang, Z. Ai, M. Cao, Y. Yan, Y. Zhao, Y. Liu, D. Wei, *J. Phys. Chem. Lett.* **2020**, *11*, 1909–1914; g) S. Ma, Y. Liu, J. Zhang, B. Xu, W. Tian, *J. Phys. Chem. Lett.* **2020**, *11*, 10504–10510; h) J. Chen, H. Tian, Z. Yang, J. Zhao, Z. Yang, Y. Zhang, M. P. Aldred, Z. Chi, *Adv. Opt. Mater.* **2021**, *9*, 2001550; i) Y. Liu, Z. Ma, J. Liu, M. Chen, Z. Ma, X. Jia, *Adv. Opt. Mater.* **2021**, *9*, 2001685; j) Q, Zhou, Y. Lei, H. Fu, *J. Mater. Chem. C* **2021**, *9*, 489–496; k) L. Biesen, D. Woschko, C. Janiak, T. J. J. Müller, *Chem. Eur. J.* **2022**, *28*, e202202579; l) T. Theiss, S. Buss, I. Maisuls, R. Lopez-Arteaga, D. Brünink, J. Kosters, A. Hepp, N. L. Doltsinis, E. A. Weiss, C. A. Strassert, *J. Am. Chem. Soc.* **2023**, *145*, 3937–3951.
[9] a) S. Choi, J. Bouffard, Y. Kim, *Chem. Sci.* **2014**, *5*, 751–755; b) S. Park, J. E. Kwon, S.-Y. Park, O.-H. Kwon, J. K. Kim, S.-J. Yoon, J. W. Chung, D. R. Whang, S. K. Park, D. K. Lee, D.-J. Jang, J. Gierschner, S. Y. Park, *Adv. Opt. Mater.* **2017**, *5*, 1700353.
[10] a) B.-K. An, D.-S. Lee, J.-S. Lee, Y.-S. Park, H.-S. Song, S. Y. Park, *J. Am. Chem. Soc.* **2004**, *126*, 10232–10233; b) A. V. Marsh, N. J. Cheetham, M. Little, M. Dyson, A. J. P. White, P. Beavis, C. N. Warriner, A. C. Swain, P. N. Stavrinou, M. Heeney, *Angew. Chem. Int. Ed.* **2018**, *57*, 10640–10645; c) H. Gao, Y. Gao, C. Wang, D. Hu, Z. Xie, L. Liu, B. Yang, Y. Ma, *ACS Appl. Mater. Interfaces* **2018**, *10*, 14956–14965; d) G. Tan, I. Maisuls, F. Strieth-Kalthoff, X. Zhang, C. Daniliuc, C. A. Strassert, F. Glorius, *Adv. Sci.* **2021**, *8*, 2101814; e) Y. Matsui, Y. Yokoyama, T. Ogaki, K. Ishiharaguchi, A. Niwa, E. Ohta, M. Saigo, K. Miyata, K. Onda, H. Naito, H. Ikeda, *J. Mater. Chem. C* **2022**, *10*, 4607–4613.
[11] a) M. Louis, R. Sethy, J. Kumar, S. Katao, R. Guillot, T. Nakashima, C. Allain, T. Kawai, R. Métivier, *Chem. Sci.* **2019**, *10*, 843–847; b) M. A. Potopnyk, D. Volyniuk, M. Ceborska, P. Cmoch, I. Hladka, Y. Danyliv, J. V. Gražulevičius, *J. Org. Chem.* **2018**, *83*, 12129–12142; c) M. A. Potopnyk, D. Volyniuk, R. Luboradzki, M. Ceborska, I. Hladka, Y. Danyliv, J. V. Gražulevičius, *J. Org. Chem.* **2019**, *84*, 5614–5626; d) Y. Liu, L. Hua, Z. Zhao, S. Ying, Z. Ren, S. Yan, *Adv. Sci.* **2021**, *8*, 2101326; e) Z.-F. Liu, L. Zeng, L.-Y. Niu, Q.-Z. Yang, *Chem. Commun.* **2023**, *59*, 2453–2456.
[12] a) Y. Dong, J. W. Y. Lam, A. Qin, Z. Li, J. Sun, H. H.-Y. Sung, I. D. Williams, B. Z. Tang, *Chem. Commun.* **2007**, 40–42; b) Y. Dong, J. W. Y. Lam, A. Qin, J. Sun, J. Liu, Z. Li, J. Sun, H. H. Y. Sung, I. D. Williams, H. S. Kwok, B. Z. Tang, *Chem. Commun.* **2007**, 3255–3257; c) R. Yoshii, A. Hirose, K. Tanaka, Y. Chujo, *J. Am. Chem. Soc.* **2014**, *136*, 18131–18139; d) N. Nirmalananthan, T. Behnke, K. Hoffmann, D. Kage, C. F. Gers-Panther, W. Frank, T. J. J. Müller, U. Resch-Genger, *J. Phys. Chem. C* **2018**, *122*, 11119–11127; e) R. D. Crocker, D. P. Pace, B. Zhang, D. J. M. Lyons, M. M. Bhadbhade, W. W. H. Wong, B. K. Mai, T. V. Nguyen, *J. Am. Chem. Soc.* **2021**, *143*, 20384–20394.
[13] a) Z. Chen, J. Zhang, M. Song, J. Yin, G.-A. Yu, S. H. Liu, *Chem. Commun.* **2015**, *51*, 326–329; b) R. Hagihara, T. Umeno, S. Ueki, D. Yoshihara, Y. Fuchi, K. Usui, M. Sakuma, K. Yamada, S. Karasawa, *Chem. Eur. J.* **2021**, *27*,3039–3046; c) M. Yamaguchi, S. Ito, A. Hirose, K. Tanaka, Y. Chujo, *Mater. Chem. Front.* **2017**, *1*, 1573–1579.

[14] a) Y. Sagara, T. Kato, *Nat. Chem.* **2009**, *1*, 605–610; b) Z. Chi, X. Zhang, B. Xu, X. Zhou, C. Ma, Y. Zhang, S. Liu, J. Xu, *Chem. Soc. Rev.* **2012**, *41*, 3878–3896; c) Y. Sagara, S. Yamane, M. Mitani, C. Weder, T. Kato, *Adv. Mater.* **2016**, *28*, 1073–1095.
[15] a) J. Wang, Z. Chai, J. Wang, C. Wang, M. Han, Q. Liao, A. Huang, P. Lin, C. Li, Q. Li, Z. Li, *Angew. Chem. Int. Ed.* **2019**, *58*, 17297–17302; b) T. Nakae, M. Nishio, T. Usuki, M. Ikeya, C. Nishimoto, S. Ito, H. Nishihara, M. Hattori, S. Hayashi, T. Yamada, Y. Yamanoi, *Angew. Chem. Int. Ed.* **2021**, *60*, 22871–22878; c) S. Ito, R. Sekine, M. Munakata, M. Yamashita, T. Tachikawa, *Chem. Eur. J.* **2021**, *27*, 13982–13990; d) R. Hertel, W. Maftuhin, M. Walter, M. Sommer, *J. Am. Chem. Soc.* **2022**, *144*, 21897–21907; e) Z. Chen, H. Qin, Y. Yin, D. Deng, S.-Y. Qin, N. Li, K. Wang, Y. Sun, *Chem. Eur. J.* **2023**, *29*, e202203797.
[16] a) Q. Yang, D. Li, W. Chi, R. Guo, B. Yan, J. Lan, X. Liu, J. Yin, *J. Mater. Chem. C* **2019**, *7*, 8244–8249; b) Y. Yin, Z. Chen, Y. Yang, G. Liu, C. Fan, S. Pu, *RSC Adv.* **2019**, *9*, 24338–24343; c) Z. Qiu, Z. Yang, W.-C. Chen, L. Xing, S. Hu, S. Ji, Q. Yang, N. Cai, X. Ouyang, Y. Huo, *J. Mater. Chem. C* **2020**, *8*, 4139–4147; d) K. Zheng, H. Chen, Y. Xiao, X. Liu, J. Yan, N. Zhang, *Chem. Eur. J.* **2021**, *27*, 14964–14970.
[17] X. Liu, M. Li, M. Liu, Q. Yang, Y. Chen, *Chem. Eur. J.* **2018**, *24*, 13197–13204.
[18] X. Cheng, Z. Wang, B. Tang, H. Zhang, A. Qin, J. Z. Sun, B. Z. Tang, *Adv. Funct. Mater.* **2018**, *28*, 1706506.
[19] Z. Zhang, X. Liu, Y. Feng, Z.-Q. Yu, L. Wang, X.-K. Ren, Y. Liu, *J. Mater. Chem. C* **2021**, *9*, 975–981.
[20] F. Khan, A. Ekbote, S. M. Mobin, R. Misra, *J. Org. Chem.* **2021**, *86*, 1560–1574.
[21] Y. Sagara, K. Takahashi, A. Seki, T. Muramatsu, T. Nakamura, N. Tamaoki, *J. Mater. Chem. C* **2021**, *9*, 1671–1677.
[22] B. Prusti, S. Tripathi, P. Sivasakthi, P. K. Samanta, M. Chakravarty, *ACS Appl. Opt. Mater.* **2023**, *1*, 889–897.
[23] a) G. Zhang, J. Lu, M. Sabat, C. L. Fraser, *J. Am. Chem. Soc.* **2010**, *132*, 2160–2162; b) S. Xu, R. E. Evans, T. Liu, G. Zhang, J. N. Demas, C. O. Trindle, C. L. Fraser, *Inorg. Chem.* **2013**, *52*, 3597–3610; c) P. Galer, R. C. Korošec, M. Vidmar, B. Šket, *J. Am. Chem. Soc.* **2014**, *136*, 7383–7394; d) L. Wang, K. Wang, B. Zou, K. Ye, H. Zhang, Y. Wang, *Adv. Mater.* **2015**, *27*, 2918–2922; e) M. Louis, A. Brosseau, R. Guillot, F. Ito, C. Allain, R. Métivier, *J. Phys. Chem. C* **2017**, *121*, 15897–15907; f) L. Wilbraham, M. Louis, D. Alberga, A. Brosseau, R. Guillot, F. Ito, F. Labat, R. Métivier, C. Allain, I. Ciofini, *Adv. Mater.* **2018**, *30*, 1800817; g) M. Louis, C. P. García, A. Brosseau, C. Allain, R. Métivier, *J. Phys. Chem. Lett.* **2019**, *10*, 4758–4762; h) M. A. Potopnyk, M. Kravets, R. Luboradzki, D. Volyniuk, V. Sashuk and J. V. Grazulevicius, *Org. Biomol. Chem.* **2021**, *19*, 406–415; i) M. A. Potopnyk, D. Volyniuk, R. Luboradzki, A. Lazauskas, J. V. Grazulevicius, *Eur. J. Org. Chem.* **2021**, *2021*, 2772–2781; j) B. Poggi, L. Bodelot, M. Louis, R. Métivier, C. Allain, *J. Mater. Chem. C* **2021**, *9*, 12111–12117.
[24] a) X. Wu, D.-G. Chen, D. Liu, S.-H. Liu, S.-W. Shen, C.-I Wu, G. Xie, J. Zhou, Z.-X. Huang, C.-Y. Huang, S.-J. Su, W. Zhu, P.-T. Chou, *J. Am. Chem. Soc.* **2020**, *142*, 7469–7479; b) R. Pashazadeh, P. Pander, A. Lazauskas, F. B. Dias, J. V. Grazulevicius, *J. Phys. Chem. Lett.* **2018**, *9*, 1172–1177; c) M. Mahmoudi, D. Gudeika, S. Kutsiy, J. Simokaitiene, R. Butkute, L. Skhirtladze, K. L. Woon, D. Volyniuk, J. V. Grazulevicius, *ACS Appl. Mater. Interfaces* **2022**, *14*, 40158–40172.
[25] a) Y.-Y. Wu, Y. Chen, G.-Z. Gou, W.-H. Mu, X.-J. Lv, M.-L. Du, W.-F. Fu, *Org. Lett.* **2012**, *14*, 5226–5229; b) H. G. Bonacorso, T. P. Calheiro, B. A. Iglesias, I. R. C. Berni, E. N. da Silva Júnior, J. B. T. Rocha, N. Zanatta, M. A. P. Martins, *Tetrahedron Lett.* **2016**, *57*, 5017–5021.
[26] a) Z. R. Grabowski, K. Rotkiewicz, W, Rettig, *Chem. Rev.* **2003**, *103,* 3899–4031; b) C. Wang, W. Chi, Q. Qiao, D. Tan, Z. Xu, X. Liu, *Chem. Soc. Rev.* **2021**, *50*, 12656–12678.
[27] Agilent Technologies, *CrysAlisPro*, Version 1.171.38.46.
[28] G. M. Sheldrick, *Acta Crystallogr. Sect. A* **2015**, *71*, 3–8.
[29] L. J. Farrugia, *J. Appl. Crystallogr.* **1999**, *32*, 837–838.
[30] M. J. Frisch, G. W. Trucks, H. B. Schlegel, G. E. Scuseria, M. A. Robb, J. R. Cheeseman, G. Scalmani, V. Barone, G. A. Petersson, H. Nakatsuji, X. Li, M. Caricato, A. V. Marenich, J. Bloino, B. G. Janesko, R. Gomperts, B. Mennucci, H. P. Hratchian, J. V. Ortiz, A. F. Izmaylov, J. L. Sonnenberg, D. Williams-Young, F. Ding, F. Lipparini, F. Egidi, J. Goings, B. Peng, A. Petrone, T. Henderson, D. Ranasinghe, V. G. Zakrzewski, J. Gao, N. Rega, G. Zheng, W. Liang, M. Hada, M. Ehara, K. Toyota, R. Fukuda, J. Hasegawa, M. Ishida, T. Nakajima, Y. Honda, O. Kitao, H. Nakai, T. Vreven, K. Throssell, J. A. Montgomery, Jr., J. E. Peralta, F. Ogliaro, M. J. Bearpark, J. J. Heyd, E. N. Brothers, K. N. Kudin, V. N. Staroverov, T. A. Keith, R. Kobayashi, J. Normand, K. Raghavachari, A. P. Rendell, J. C. Burant, S. S. Iyengar, J. Tomasi, M. Cossi, J. M. Millam, M. Klene, C. Adamo, R. Cammi, J. W. Ochterski, R. L. Martin, K. Morokuma, O. Farkas, J. B. Foresman and D. J. Fox, *Gaussian 16*, Gaussian, Inc., Wallingford CT, **2016**.
[31] a) W.-F. Fu, L.-F. Jia, W.-H. Mu, X. Gan, J.-B. Zhang, P.-H. Liu, Q.-Y. Cao, G.-J. Zhang, L. Quan, X.-J. Lv, Q.-Q. Xu, *Inorg. Chem.* **2010**, *49*, 4524–4533; b) Z. Li, W. Zhao, X. Li, Y. Zhu, C. Liu, L. Wang, M. Yu, L. Wei, M. Tang, H. Zhang, *Inorg. Chem.* **2012**, *51*, 12444–12449.
[32] I. B. Berlman, *Handbook of fluorescence spectra of aromatic molecules.* New York: Academic Press, **1971**.
[33] M.-L. Du, C.-Y. Hu, L.-F. Wang, C. Li, Y.-Y. Han, X. Gan, Y. Chen, W.-H. Mu, M. L. Huang, W.-F. Fu, *Dalton Trans.* **2014**, *43*, 13924–13931.
[34] G. Angulo, G. Grampp, A. Rosspeintner, *Spectrochim. Acta Part A* **2006**, *65*, 727–731.
[35] S. J. Strickler, R. A. Berg, *J. Chem. Phys.* **1962**, *37*, 814–822.
[36] N. C. Greenham, I. D. W. Samuel, G. R. Hayes, R. T. Phillips, Y. A. R. R. Kessener, S. C. Moratti, A. B. Holmes, R. H. Friend, *Chem. Phys. Lett.* **1995**, *241*, 89–96.
[37] J. A. Gardecki, M. Maroncelli, *Appl. Spectrosc.* **1998**, *52*, 1179–1189.
[38] T. S. Ahn, R. O. Al-Kaysi, A. M. Müller, K. M. Wentz, C. J. Bardeen, *Rev. Sci. Instrum.* **2007**, *78*, 086105.
[39] a) W. Siebrand, T. A. Wildman, *Acc. Chem. Res.* **1986**, *19*, 238–243; b) A. Plonka, *Annu. Rep. Prog. Chem. Sect. C* **2001**, *97*, 91–147.
[40] M. N. Berberan-Santos, E. N. Bodunov, B. Valeur, *Chem. Phys.* **2005**, *317*, 57–62.
[41] M. N. Berberan-Santos, E. N. Bodunov, B. Valeur, *Chem. Phys.* **2005**, *315*, 171–182.

Manuscript received: January 2, 2024
Accepted manuscript online: February 16, 2024
Version of record online: ■■, ■■

RESEARCH ARTICLE

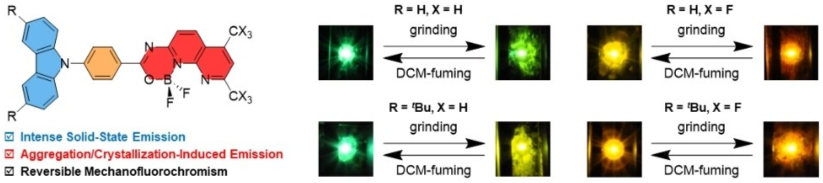

Four solid-state luminescent donor-acceptor boron difluoride complexes based on the carbazole electron donor and [1,3,5,2]oxadiazaborinino[3,4-*a*][1,8]naphthyridine acceptor were designed and synthesized. These dyes exhibit aggregation-induced emission and reversible mechanofluorochromism. The incorporation of CF_3-groups into naphthyridine unit provide the crystallization-induced emission enhancement of the dyes.

Dr. M. A. Potopnyk, Dr. J. Mech-Piskorz, Dr. G. Angulo*, Dr. M. Ceborska, Dr. R. Luboradzki, Dr. E. Andresen, Dr. A. Gajek, Dr. A. Wisniewska, Dr. U. Resch-Genger**

1 – 12

Aggregation/Crystallization-Induced Emission in Naphthyridine-Based Carbazolyl-Modified Donor-Acceptor Boron Dyes Tunable by Fluorine Atoms